Title

Dynamic Contrast-Enhanced MRI in Abdominal Aortic Aneurysms as a Potential Marker for Disease Progression.

Journal

Journal of Magnetic Resonance Imaging, 58(4)

Authors

Zhou, Ang
Leach, Joseph
Zhu, Chengcheng
et al.

Publication Date

2023-10-01

DOI

10.1002/jmri.28640

Peer reviewed

U.S. Department of Veterans Affairs
Public Access Author manuscript
J Magn Reson Imaging. Author manuscript; available in PMC 2025 January 16.

Published in final edited form as:
J Magn Reson Imaging. 2023 October ; 58(4): 1258–1267. doi:10.1002/jmri.28640.

Dynamic Contrast-Enhanced MRI in Abdominal Aortic Aneurysms as a Potential Marker for Disease Progression

Ang Zhou, PhD[1,3], **Joseph R Leach, MD, PhD**[1,3], **Chengcheng Zhu, PhD**[4], **Huiming Dong, PhD**[1,3], **Fei Jiang, PhD**[5], **Yoo Jin Lee, MD**[1], **James Iannuzzi, MD, MPH**[2,3], **Warren Gasper, MD**[2,3], **David Saloner, PhD**[1,3], **Michael D Hope, MD**[1,3], **Dimitrios Mitsouras, PhD**[1,3]

[1]Department of Radiology and Biomedical Imaging, University of California San Francisco, San Francisco, USA

[2]Department of Surgery, University of California San Francisco, San Francisco, USA

[3]San Francisco Veterans Affairs Medical Center, San Francisco, USA

[4]Department of Radiology, University of Washington, Seattle, USA

[5]Department of Biostatistics, University of California San Francisco, San Francisco, USA

Abstract

Background: Abdominal aortic aneurysms (AAAs) may rupture before reaching maximum diameter (D_{max}) thresholds for repair. Aortic wall microvasculature has been associated with elastin content and rupture sites in specimens, but its relation to progression is unknown.

Purpose: To investigate whether dynamic contrast-enhanced (DCE) MRI of AAA is associated with D_{max} or growth.

Study Type: Prospective.

Population: 27 male patients with infrarenal AAA (mean age±standard deviation=75±5 years) under surveillance with DCE MRI and two years of prior follow-up intervals with computed tomography (CT) or MRI.

Field Strength/Sequence: 3-T, dynamic three-dimensional (3D) fast gradient-echo stack-of-stars volumetric interpolated breath-hold examination (Star-VIBE).

Assessment: Wall voxels were manually segmented in 2 consecutive slices at the level of D_{max}. We measured slope to 1-min and area under the curve (AUC) to 1- and 4-min of the signal intensity change post-contrast relative to that pre-contrast arrival, and, K^{trans}, a measure of microvascular permeability, using the Patlak model. These were averaged over all wall voxels for association to Dmax and growth rate, and, over left/right and anterior/posterior quadrants for testing circumferential homogeneity. D_{max} was measured orthogonal to the aortic centerline and growth rate was calculated by linear fit of D_{max} measurements.

Corresponding Author Information: Dimitrios Mitsouras, PhD, Address: 4150 Clement Street, Box 114, San Francisco, CA 94121, USA, Tel: 415.221.4810, dimitrios.mitsouras@ucsf.edu.

Statistical Tests: Pearson correlation and linear mixed effects models. A P-value <0.05 was considered statistically significant.

Results: In 44 DCE MRIs, mean D_{max} was 45±7 mm and growth rate in 1.5±0.4 years of prior follow-up was 1.7±1.2 mm per year. DCE measurements correlated with each other (Pearson r=0.39-0.99) and significantly differed between anterior/posterior versus left/right quadrants. DCE measurements were not significantly associated with D_{max} (P=0.084, 0.289, 0.054 and 0.255 for slope, AUC at 1- and 4-min, and K^{trans}, respectively). Slope and 4-min AUC significantly associated with growth rate after controlling for D_{max}.

Conclusion: Contrast uptake may be increased in lateral aspects of the AAA. Contrast enhancement 1-min slope and 4-min AUC may be associated with a period of recent AAA growth that is independent of D_{max}.

Keywords

Abdominal Aortic Aneurysm; Dynamic Contrast-Enhanced MRI; Microvasculature; Vessel Wall Imaging

Introduction

Abdominal aortic aneurysm (AAA), a pathologic dilatation of the abdominal aorta to greater than 3 cm in diameter, has a pooled global prevalence of 4.8% (1). Rupture as the major complication of unrepaired AAAs has an overall mortality rate of up to 80%-90% (2). Maximum diameter of AAAs is the best known predictor of rupture risk and is the primary metric used to time elective open or endovascular repair, which is generally recommended at diameters >5.5 cm in men and >5.0 cm in women (3). Earlier elective repair of small AAA (4-5.5 cm) may not confer a net mortality benefit (4). Nonetheless, maximum aortic diameter is an imprecise predictor of rupture risk and up to 40% of ruptured AAAs are below repair thresholds at last surveillance (5, 6). Improved AAA risk stratification thus remains a relevant need.

Inflammation is a central process in the development and progression of AAAs and is believed to have a substantial impact on the degradation and weakening of the aortic wall (7). Despite considerable efforts to improve risk stratification by imaging inflammation of the AAA wall (8, 9), no widely available clinical tools have yet emerged. Recently, dynamic contrast-enhanced (DCE) MRI has been proposed for the imaging of AAAs (10, 11). Specifically, DCE MRI is a well-established technique that enables to quantify the kinetics of gadolinium-based contrast agent uptake in tissues (12–14). Various measurements obtained from DCE MRI have been shown to have a quantitative relationship with microvascular density and macrophage accumulation in human and animal atherosclerotic lesions (14). The use of DCE MRI for imaging of AAAs is motivated by the role of microvasculature as a source of inflammatory cells that express matrix metalloproteinases that can contribute to aneurysm wall weakening (15), and the increased neovascularization observed at rupture sites (16). To date, DCE MRI of the AAA wall has been shown to be feasible and reproducible (10, 11). However, its potential relationship to inflammation and its role with respect to AAA progression risk is unknown.

Against this background, the first aim of this study was to determine the extent to which the AAA wall exhibits heterogeneous contrast uptake in DCE MRI studies. Second, we aimed to determine whether DCE measurements of the AAA wall are associated with maximum diameter or recent progression.

Material and Methods

This single-center study was approved by the Institutional Review Board and was compliant with the Health Insurance Portability and Accountability Act (HIPAA).Written informed consent was obtained for all patients except when the IRB waived the requirement for informed consent on the basis of retrospective review of existing clinical data.

Study Population

Patients with infrarenal AAAs under imaging surveillance with at least one abdominal computed tomography (CT) or three-dimensional (3D) MRI study in the preceding 2 years were prospectively enrolled at a single center. In keeping with prior work, patients that did not have at least 2 voxels of intraluminal thrombus allowing clear separation of the aortic wall and lumen so as to allow for DCE analyses were excluded (10, 11). Twenty-seven AAA patients (all male; mean age: 75±5.3 years, range: 64-87 years), who underwent a total of 44 DCE MRI scans between March 2019 and May 2022, were thus included in this study. The enrollment flow chart is shown in Figure 1 and detailed demographic information on all patients is shown in Table 1.

MRI Protocol

All MRI scans were acquired on a 3-Tesla whole body system (Magnetom Skyra, Siemens Healthineers, Erlangen, Germany) using a 16-channel chest array. Twenty time points (dynamic phases) were acquired using a three-dimensional (3D) fast gradient-echo stack-of-stars volumetric interpolated breath-hold examination (Star-VIBE) sequence with a temporal resolution of 13-15 s per phase for 20-26 axial slices covering the AAA sac. Other sequence parameters were as follows: 5 mm slice thickness, 240 mm field of view and 224 radial spokes reconstructed at 176x176 matrix size, repetition time (TR)/echo time (TE) = 2.7-3.9/1.3-1.9 ms, flip angle 7-9°. The total acquisition time was approximately 5-7 minutes. During acquisition of the dynamic series, 20 ml of 1:1 mixture of Gadovist (1 mmol/ml; Bayer Schering Pharma AG, Berlin, Germany) and saline were injected in the antecubital vein with a power injector (MEDRAD Spectris Solaris, Bayer HealthCare LLC, Whippany, NJ, USA) at a rate of 2 ml/sec, followed by 15 ml of saline injected at 2 ml/sec.

DCE Analysis

The DCE images at each time point were co-registered to the initial time point using commercial software (Tissue 4D, version 1.0; Siemens Healthineers, Erlangen, Germany) to minimize errors due to motion during the prolonged acquisition. For the purposes of this work, we analyzed two consecutive axial slices near the location of AAA maximum diameter, where the aneurysm wall was clearly visible. The AAA lumen and wall in each slice were manually segmented using the open-source medical image software Horos (version 3.3.6; https://horosproject.org/) by two vascular imaging scientists in consensus

(_._. with 3 years of experience, and _._. with 5 years of experience) under the supervision of a board-certified abdominal radiologist (_._.) with 9 years of experience. The two imaging scientists additionally independently segmented a subset of 10 DCE MRI studies >6 months after the consensus segmentation to minimize the opportunity for study recall.

The relative enhancement of each voxel within the AAA through time was calculated as the ratio of signal intensity after contrast arrival to that before contrast arrival (17). We then calculated the area under the curve (AUC) for normalized relative enhancement at 1 min and 4 min after contrast arrival, as well as the slope of contrast enhancement over the first minute after contrast arrival. For these model-free measurements, we first normalized the relative enhancement curve at each voxel by dividing by the peak luminal enhancement to mitigate inter-patient variability not related to the AAA, such as from differences in cardiac output or flow distribution (18).

Contrast agent kinetics within each mural voxel were quantified with a custom-made program implemented in Python (version 3.6; http://www.python.org/) using the Patlak model (12). This yielded the volume transfer constant of contrast agent from blood plasma to the extracellular extravascular space (K^{trans}, a parameter with direct but mixed dependence on microvascular flow, permeability, and surface area), and the volume of blood plasma space per unit volume of tissue (v_p) in the following equation:

$$C_t(t) = v_p C_p(t) + K^{trans} \int_o^t C_p(\tau) d\tau,$$

where $C_t(t)$ is time-dependent contrast concentration in the vessel wall tissue calculated from the un-normalized relative enhancement curves, and $C_p(t)$ is the contrast concentration in blood plasma. The T1 relaxation time of the AAA wall was assumed to be 1,230 ms based on measurements performed in aortic wall tissue specimens at 3 T at our institution, and a generalized arterial input function (AIF) previously measured for AAA by Nguyen *et al.* (11) was used for $C_p(t)$.

For statistical analyses described below, the pixel-wise AUC, slope, and K^{trans} were averaged over all pixels belonging to the segmented wall in the two consecutive slices analyzed. In addition, to investigate the distribution of the different metrics (AUC, slope, K^{trans}) around the aneurysm circumference, measurements were also averaged from all pixels in the two slices but in each of four quadrants of the wall independently (left, anterior, right and posterior, Figure 2b).

Maximum Diameter of AAA and 2-year Growth Rate Calculations

The two cardiovascular imaging scientists (_._ and _._) independently measured maximum AAA diameter (D_{max}) orthogonal to the vessel centerline using commercial 3D software (Vitrea, version 7.14; Vital Images Inc., Minnetonka, MN, USA) in all DCE MRI studies as well as in CT and non-DCE MRI studies used as priors. In MRI studies, Dmax was measured from a high-resolution, 1.25 mm isotropic 3D post-contrast Star-VIBE acquisition acquired as part of the standard AAA surveillance protocol at our institution, as previously

described (19). In CT studies, Dmax was measured from images reconstructed with a soft tissue kernel at 1.25 mm slice thickness and 0.7 mm in-plane resolution. Growth rate leading up to each DCE scan was calculated using linear regression of D_{max} measurements in all CT and MRI studies of the patient available in the hospital electronic medical recordsin the 2-year period preceding the DCE scan. All AAA patients at our institution typically have a surveillance imaging study, primarily by MRI, every 6 to 12 months depending on AAA diameter.

Statistical Analysis

Statistical analyses were performed using Stata (version 12.1, StataCorp, College Station, TX, USA). To quantify the inter-observer variability of the slope, AUC and K^{trans} DCE measurements as well as of Dmax measurements by the two readers, we reported the mean of the pair wise differences (bias) with 95% confidence intervals (limits of agreement; LOA), as well as the intraclass correlation coefficient (ICC) and the percent coefficient of variation (CoV; CoV = within-subject standard deviation / mean measurement × 100%).

All subsequent statistical analyses were based on the slope, AUC and K^{trans} DCE measurements resulting from the consensus segmentation of the aortic wall, and the Dmax measured by the more experienced reader (_._). To test the homogeneity of slope, AUC and K^{trans} measurements, based on a previous report of the higher microvascular density in lateral aspects of AAA (20), we studied the difference between the average left-right and average anterior-posterior values of each measurement. To do so, we built a linear mixed effects model for the value of each measurement and the corresponding side of the measurement, using the anterior-posterior side as the reference group without loss of generality. The models considered the measurements from the same patient at the same time to share the same random effect.

To test the association of the slope, AUC and K^{trans} DCE measurements with the outcome variables of D_{max} and fitted growth rate, we built linear mixed effects models considering data from the same patient to share the same random effect. Similar linear mixed effects models were also built to test the association of the DCE measurements on growth rate while also controlling for D_{max}, again considering data from the same patient to share the same random effect. For each of these models we reported the P-values of the predictor for each outcome, and whenever the P-value was significant, the estimated effect size and 95% confidence interval (C.I.) Finally, we tested the correlation of DCE measurements to each other using Pearson's correlation coefficient. A P-value <0.05 was considered statistically significant.

Results

Amongst the 27 patients, 17 had a single DCE MRI study, 5 had 2 studies, 4 had 3 studies, and 1 patient had 5 studies. Across all DCE MRI studies, the mean wall AUC was 23.7±14.2 s and 182.4±88.7 s at 1 and 4 min, respectively, the mean slope was 0.011±0.006 s^{-1}, and the mean K^{trans} was 0.040±0.026 min^{-1}. Figure 2 shows the mean relative enhancement of the AAA wall and lumen and the voxel-wise 4 min AUC, slope, and K^{trans} maps for a

representative slow-growing AAA (growth rate of 1 mm/year), and Figure 3 shows these measures for a representative faster-growing AAA (growth rate of 5 mm/year).

Figure 4 presents all 1 min and 4 min AUC, slope, and K^{trans} measurements of the entire AAA wall, each quadrant individually, as well as the minimum and maximum values across the four quadrants for each DCE MRI scan. All measurements exhibited a statistically significant difference between the lateral aspects and the anterior/posterior aspects of the AAA (Table 2). Specifically, the estimated effect of lateral aspects on DCE measurements were an 18.2% increase in slope, a 19.5% increase in K^{trans}, and a 13.2% and 13.7% increase in 1 min and 4 min AUC, respectively (Table 2).

The average AAA maximum diameter in the 44 DCE MRI studies was 45±7 mm. The patients underwent a total of 107 CT/MR imaging studies (16 by CT) in the 2 years leading up to and including all the DCE MRI studies. On average, 3.3±1.2 imaging studies were available in the 2 years prior to each DCE MRI study for growth rate calculation, reflecting a roughly 6-month follow-up interval for these AAAs under routine surveillance. According to those studies, the average follow-up interval leading up to the DCE MRIs for growth rate calculation was 1.5±0.4 years, and the average aneurysm growth rate observed in that interval was 1.7±1.2 mm per year. None of the DCE measurements had a statistically significant association with D_{max} (AUC at 1 min, P =0.289, Figure 5a; AUC at 4 min, P = 0.054; slope, P = 0.084, Figure 5c; and K^{trans}, P = 0.255, Figure 6a). The growth rate had a statistically significant association with AUC at 4 min (effect size = 0.005, 95% C.I.: [0.001 – 0.009]) and with slope (effect size = 79.99, 95% C.I.: [19.69 – 140.3]), which is shown in Figure 5d. No significant effect on growth rate was observed for AUC at 1 min (P = 0.297, Figure 5b) or K^{trans} (P = 0.696, Figure 6b). After controlling for D_{max}, the effect of slope and 4 min AUC on growth rate remained statistically significant (Table 3), with a 0.01 s^{-1} increase in slope and a 171.7 s increase in 4 min AUC each associated with a 1 mm/year faster growth rate that was independent of AAA maximum diameter (Table 3).

Finally, all four DCE metrics had statistically significant correlations with each other. Specifically, K^{trans} was moderately correlated with slope (r = 0.59) and AUC (r=0.39 and 0.62 at 1 and 4 min, respectively). Slope was strongly correlated with AUC at 1 min (r = 0.92) and with AUC at 4 min (r = 0.99).

Interobserver Agreement

The bias, limits of agreement and coefficient of variation according to the DCE analysis of 10 studies independently segmented by 2 readers are presented in Table 4. The ICC was high for all DCE measurements: 99.1% with 95% C.I. of [96.7% – 99.7%] for the slope, 99.2% with 95% C.I. of [96.7% – 99.8%] for the AUC at 1 min, 99.2% with 95% C.I. of [97.0% – 99.9%] for the AUC at 4 min, and 99.7% with 95% C.I. of [98.4% – 99.9%] for K^{trans}.

The bias, limits of agreement and coefficient of variation for Dmax across all 107 CT/MRI studies measured by the two independent readers were −0.34 mm, [−2.73 – 2.05] mm and 1.45%, respectively, while the ICC was 98.5% with 95% C.I. of [97.1% – 99.2%]. When using the second reader's Dmax measurements and growth rates resulting from those measurements, the findings were identical to those using the first reader's measurements.

Specifically, there was no statistically significant association between Dmax and DCE measurements (P=0.132, P=0.867, P=0.150 and P=0.887 for slope, AUC at 1 and 4 min and K^{trans}, respectively) or between growth rate and AUC at 1 min (P=0.150) and K^{trans} (P=0.270). Statistically significant associations were again observed between growth rate and slope and AUC at 4 min that persisted after controlling for Dmax.

Discussion

In this study, the DCE measurements explored, namely normalized relative enhancement slope to 1 min, AUC to 1 min and 4 min, and K^{trans}, were highly reproducible by different readers and exhibited differences between the lateral and the anterior and posterior aspects of AAA. Furthermore, our findings suggest that characterization of contrast kinetics, specifically the initial enhancement slope and late AUC, may offer information about aneurysm progression independent from maximal diameter.

Improved AAA risk stratification could be valuable toward optimizing surveillance intervals and timing prophylactic elective repair for a large number of patients. Owing to its potential to assess mural microvasculature, DCE MRI could offer AAA characterization more biologically meaningful than maximal aneurysm diameter, the primary aneurysm feature currently used for risk assessment and clinical management. Increased AUC and K^{trans} have been previously linked to increased microvascular density in atherosclerotic lesions (21, 22). Both metrics have also been found to change in response to vessel wall injury or anti-inflammatory therapies (23–25) and in tandem with underlying changes in either microvascular density or microvascular permeability (26, 27).

Typically, AAAs have more than a 10-fold higher microvascular density compared to normal aortas, which is also about 3-fold higher than that of normal-caliber atherosclerotic aortas (28, 29). This extensive microvasculature may help to recruit and transport inflammatory cells that express matrix metalloproteinases that contribute to AAA wall destabilization (30). Furthermore, cells lining both mature and immature microvessels in AAAs are equally relevant sources of matrix metalloproteinases as macrophages and other inflammatory infiltrates (15). Rupture edges of AAAs may also exhibit a high density of immature, more permeable microvessels, and overexpression of proangiogenic cytokines indicating active, ongoing angiogenesis (16). Moreover, regardless of the mode by which the microvasculature and its permeability contribute to AAA wall destabilization, heavily vascularized regions of the media contain reduced load-bearing elastic tissue (15), thus motivating the in vivo quantification of the microvasculature toward risk stratification.

The heterogeneity of DCE measurements that we observed around the AAA wall circumference may indirectly establish an association to inflammation (20). Specifically, we found that the lateral aspects of AAAs exhibited faster and stronger contrast uptake, as quantified by the normalized slope and AUC respectively, as well as increased K^{trans}. In histology, the lateral sites of AAA have been shown to have on average 25% higher microvascular density accompanied by a 3-fold larger area of the AAA wall covered by inflammatory infiltrates compared to the anterior and posterior sites (20). In our study, the difference in DCE measurements between lateral versus anterior/posterior sides had a

similar magnitude to the histologic difference in microvascular density, particularly for slope and K^{trans}.

Previously, Nguyen et al. showed that DCE MRI of the AAA wall is feasible and that wall AUC and K^{trans} have good inter-/intra-observer and scan-rescan reproducibility (10). This seems similar to findings in the carotids (22, 31). We also found excellent interobserver agreement of DCE measurements. With regards to the association of DCE measurements with AAA progression risk, K^{trans} calculated using the Patlak pharmacokinetic model has been shown to be weakly to moderately associated with maximum AAA diameter, but the statistical significance of the association was lost when using the Tofts or Extended Tofts models (10, 11). That group also found that initial 1 min AUC was not associated with D_{max} and that late 5 min AUC trended toward a weak correlation with it (10). Our results are in agreement with prior work for AUC (10), but not for K^{trans} (10, 11), despite using the Patlak model as well. Differences in our findings regarding K^{trans} can arise from a number of factors, including our use of a different (3D) acquisition protocol, higher temporal resolution (13 s for the majority of studies), and higher effective injection rate (1 mmol/s) in the present study. Conversely, model-free parameters such as the AUC calculated from the course of contrast uptake may be less sensitive to some of these factors.

The present work may help to establish a more direct association between DCE measurements and AAA progression. Specifically, we found that the 4 min AUC as well as the initial slope were associated with aneurysm growth in an average of 1.5 year follow-up interval preceding the DCE study. Importantly, this effect remained statistically significant after controlling for AAA maximum diameter. Although DCE measurements including K^{trans} do not have simple interpretations (13, 32, 33), the initial part of the contrast enhancement curve is influenced by the tissue perfusion flow rate (32). The association of growth rate with initial slope observed may thus suggest that AAAs experiencing a period of faster growth in our study may have more extensive microvasculature. This interpretation is consistent with previous work in tumors that has found that initial slope is determined by microvascular density and distribution (34), more so than the initial AUC (35). Initial slope is now studied as a promising parameter for improving cancer detection as it only requires short (<100 sec), though high temporal resolution DCE MRI studies (36, 37).

Unfortunately, there are no previous studies of initial slope in either atherosclerotic lesions or AAA to compare our findings with. However, we found that the initial slope was strongly correlated to the 4 min AUC, suggesting that in AAA, both measurements provide nearly identical information. Thus, if our findings are further confirmed, concentrating on initial slope may allow short DCE MRI studies for AAA risk stratification, as initial slope to 1 min and AUC to 4 min were the only two parameters we found to have an association with growth rate. An abbreviated 60-100 sec DCE MRI scan to obtain only slope is preferable in a busy clinical setting and may also pose fewer challenges (e.g., due to patient motion in-between dynamic phases, which is expected to be larger over the course of a few minutes).

Limitations

Limitations of this study include the small sample size and the lack of a control group or DCE measurements in unaffected aortic wall. Due to practice conditions in the Veterans

Affairs health care system, only male patients were included in this study. Nonetheless, the prevalence of AAA in males compared to females is 4:1 (38) so that our findings could remain applicable to a relevant proportion of the affected population. Second, this was a single-center study, which can affect reproducibility and accuracy of the measurements due to the institution-specific imaging protocols and expertise.

In this study we employed DCE MRI techniques that have been previously successfully used for the study of AAA (10, 11, 31). These include use of an in-plane acquired image resolution of <1.5 mm and <6 mm slice thickness (10, 11) and a fixed tissue pre-bolus T1 relaxation time for estimating contrast concentration (10, 11, 31) that may allow reproducible analysis of the AAA wall contrast enhancement. Similarly, for K^{trans} calculation we used a population-average AIF previously reported for AAA (10, 31) and the Patlak model that has been generally found to be better-suited for vessel wall analyses (11, 31). Further improvements are nonetheless possible. These include for example higher temporal resolution (< 5 sec) to allow capturing each individual patient's AIF (10) and concurrent tissue T1 mapping to that may further increase the accuracy of tissue contrast concentration quantification. Similarly, higher in-plane spatial resolution (<1 mm) may help minimize partial volume effects given the 1-2.5 mm thickness of the AAA vessel wall (39). New DCE MRI techniques such as multitasking (40) and compressed sensing (36) can potentially offer these improvements and should thus be researched in the future.

Importantly, our results only support that DCE MRI measurements are associated with a recent period of AAA growth independent of maximum AAA diameter, since we only considered AAA growth over the 2 year interval preceding each DCE MRI study. Prospective studies with long patient follow-up periods are needed to establish whether DCE MRI is similarly associated with future AAA progression. Finally, correlative histology will be needed to directly establish the association of the DCE measurements with microvascular density and inflammation of the aneurysm wall.

Conclusion

Quantitative measurements of dynamic contrast enhancement, specifically initial slope and late AUC may be associated with recent AAA growth rate independent of AAA maximum diameter.

Grant Support

VA Merit Award I01-CX002071

References

1. Li X, Zhao G, Zhang J, Duan Z, Xin S. Prevalence and trends of the abdominal aortic aneurysms epidemic in general population--a meta-analysis. PLoS One. 2013;8(12):e81260. [PubMed: 24312543]
2. Bengtsson H, Bergqvist D. Ruptured abdominal aortic aneurysm: a population-based study. J Vasc Surg. 1993;18(1):74–80. [PubMed: 8326662]

3. Chaikof EL, Dalman RL, Eskandari MK, et al. The Society for Vascular Surgery practice guidelines on the care of patients with an abdominal aortic aneurysm. J Vasc Surg. 2018;67(1):2–77 e2. [PubMed: 29268916]

4. Powell JT, Brown LC, Forbes JF, et al. Final 12-year follow-up of surgery versus surveillance in the UK Small Aneurysm Trial. Br J Surg. 2007;94(6):702–8. [PubMed: 17514693]

5. Ahmad M, Mistry R, Hodson J, Bradbury AW. How Quickly Do Asymptomatic Infrarenal Abdominal Aortic Aneurysms Grow and What Factors Affect Aneurysm Growth Rates? Analysis of a Single Centre Surveillance Cohort Database. Eur J Vasc Endovasc Surg. 2017;54(5):597–603. [PubMed: 28882515]

6. Brown LC, Powell JT. Risk factors for aneurysm rupture in patients kept under ultrasound surveillance. UK Small Aneurysm Trial Participants. Ann Surg. 1999;230(3):289–96; discussion 96-7. [PubMed: 10493476]

7. Thompson RW, Geraghty PJ, Lee JK. Abdominal aortic aneurysms: basic mechanisms and clinical implications. Curr Probl Surg. 2002;39(2):110–230. [PubMed: 11884965]

8. Jalalzadeh H, Indrakusuma R, Planken RN, Legemate DA, Koelemay MJ, Balm R. Inflammation as a Predictor of Abdominal Aortic Aneurysm Growth and Rupture: A Systematic Review of Imaging Biomarkers. Eur J Vasc Endovasc Surg. 2016;52(3):333–42. [PubMed: 27283346]

9. MA3RS Study Investigators. Aortic Wall Inflammation Predicts Abdominal Aortic Aneurysm Expansion, Rupture, and Need for Surgical Repair. Circulation. 2017;136(9):787–97. [PubMed: 28720724]

10. Nguyen VL, Backes WH, Kooi ME, et al. Quantification of abdominal aortic aneurysm wall enhancement with dynamic contrast-enhanced MRI: feasibility, reproducibility, and initial experience. J Magn Reson Imaging. 2014;39(6):1449–56. [PubMed: 24151142]

11. Nguyen VL, Kooi ME, Backes WH, et al. Suitability of pharmacokinetic models for dynamic contrast-enhanced MRI of abdominal aortic aneurysm vessel wall: a comparison. PLoS One. 2013;8(10):e75173. [PubMed: 24098370]

12. Patlak CS, Blasberg RG, Fenstermacher JD. Graphical evaluation of blood-to-brain transfer constants from multiple-time uptake data. J Cereb Blood Flow Metab. 1983;3(1):1–7. [PubMed: 6822610]

13. Sourbron SP, Buckley DL. On the scope and interpretation of the Tofts models for DCE-MRI. Magn Reson Med. 2011;66(3):735–45. [PubMed: 21384424]

14. van Hoof RH, Heeneman S, Wildberger JE, Kooi ME. Dynamic Contrast-Enhanced MRI to Study Atherosclerotic Plaque Microvasculature. Curr Atheroscler Rep. 2016;18(6):33. [PubMed: 27115144]

15. Reeps C, Pelisek J, Seidl S, et al. Inflammatory infiltrates and neovessels are relevant sources of MMPs in abdominal aortic aneurysm wall. Pathobiology. 2009;76(5):243–52. [PubMed: 19816084]

16. Choke E, Thompson MM, Dawson J, et al. Abdominal aortic aneurysm rupture is associated with increased medial neovascularization and overexpression of proangiogenic cytokines. Arterioscler Thromb Vasc Biol. 2006;26(9):2077–82. [PubMed: 16809548]

17. Calcagno C, Lobatto ME, Dyvorne H, et al. Three-dimensional dynamic contrast-enhanced MRI for the accurate, extensive quantification of microvascular permeability in atherosclerotic plaques. NMR Biomed. 2015;28(10):1304–14. [PubMed: 26332103]

18. Bae KT. Intravenous contrast medium administration and scan timing at CT: considerations and approaches. Radiology. 2010;256(1):32–61. [PubMed: 20574084]

19. Zhu C, Tian B, Leach JR, et al. Non-contrast 3D black blood MRI for abdominal aortic aneurysm surveillance: comparison with CT angiography. Eur Radiol. 2017;27(5):1787–94. [PubMed: 27553926]

20. Hurks R, Pasterkamp G, Vink A, et al. Circumferential heterogeneity in the abdominal aortic aneurysm wall composition suggests lateral sides to be more rupture prone. J Vasc Surg. 2012;55(1):203–9. [PubMed: 21944916]

21. Calcagno C, Cornily JC, Hyafil F, et al. Detection of neovessels in atherosclerotic plaques of rabbits using dynamic contrast enhanced MRI and 18F-FDG PET. Arterioscler Thromb Vasc Biol. 2008;28(7):1311–7. [PubMed: 18467641]

22. Kerwin WS, Oikawa M, Yuan C, Jarvik GP, Hatsukami TS. MR imaging of adventitial vasa vasorum in carotid atherosclerosis. Magn Reson Med. 2008;59(3):507–14. [PubMed: 18306402]
23. Chen H, Ricks J, Rosenfeld M, Kerwin WS. Progression of experimental lesions of atherosclerosis: assessment by kinetic modeling of black-blood dynamic contrast-enhanced MRI. Magn Reson Med. 2013;69(6):1712–20. [PubMed: 22829477]
24. Dong L, Kerwin WS, Chen H, et al. Carotid artery atherosclerosis: effect of intensive lipid therapy on the vasa vasorum--evaluation by using dynamic contrast-enhanced MR imaging. Radiology. 2011;260(1):224–31. [PubMed: 21493792]
25. Vucic E, Dickson SD, Calcagno C, et al. Pioglitazone modulates vascular inflammation in atherosclerotic rabbits noninvasive assessment with FDG-PET-CT and dynamic contrast-enhanced MR imaging. JACC Cardiovasc Imaging. 2011;4(10):1100–9. [PubMed: 21999870]
26. van Hoof RHM, Hermeling E, Sluimer JC, et al. Heart rate lowering treatment leads to a reduction in vulnerable plaque features in atherosclerotic rabbits. PLoS One. 2017;12(6):e0179024. [PubMed: 28640847]
27. Vucic E, Calcagno C, Dickson SD, et al. Regression of inflammation in atherosclerosis by the LXR agonist R211945: a noninvasive assessment and comparison with atorvastatin. JACC Cardiovasc Imaging. 2012;5(8):819–28. [PubMed: 22897996]
28. Holmes DR, Liao S, Parks WC, Thompson RW. Medial neovascularization in abdominal aortic aneurysms: a histopathologic marker of aneurysmal degeneration with pathophysiologic implications. J Vasc Surg. 1995;21(5):761–71; discussion 71-2. [PubMed: 7539511]
29. Thompson MM, Jones L, Nasim A, Sayers RD, Bell PR. Angiogenesis in abdominal aortic aneurysms. Eur J Vasc Endovasc Surg. 1996;11(4):464–9. [PubMed: 8846184]
30. Shah PK. Inflammation, metalloproteinases, and increased proteolysis: an emerging pathophysiological paradigm in aortic aneurysm. Circulation. 1997;96(7):2115–7. [PubMed: 9337176]
31. Gaens ME, Backes WH, Rozel S, et al. Dynamic contrast-enhanced MR imaging of carotid atherosclerotic plaque: model selection, reproducibility, and validation. Radiology. 2013;266(1):271–9. [PubMed: 23151823]
32. Cuenod CA, Balvay D. Perfusion and vascular permeability: basic concepts and measurement in DCE-CT and DCE-MRI. Diagn Interv Imaging. 2013;94(12):1187–204. [PubMed: 24211260]
33. Walker-Samuel S, Leach MO, Collins DJ. Evaluation of response to treatment using DCE-MRI: the relationship between initial area under the gadolinium curve (IAUGC) and quantitative pharmacokinetic analysis. Phys Med Biol. 2006;51(14):3593–602. [PubMed: 16825751]
34. Buadu LD, Murakami J, Murayama S, et al. Breast lesions: correlation of contrast medium enhancement patterns on MR images with histopathologic findings and tumor angiogenesis. Radiology. 1996;200(3):639–49. [PubMed: 8756909]
35. Mori N, Abe H, Mugikura S, et al. Ultrafast Dynamic Contrast-Enhanced Breast MRI: Kinetic Curve Assessment Using Empirical Mathematical Model Validated with Histological Microvessel Density. Acad Radiol. 2019;26(7):e141–e9. [PubMed: 30269956]
36. Honda M, Kataoka M, Onishi N, et al. New parameters of ultrafast dynamic contrast-enhanced breast MRI using compressed sensing. J Magn Reson Imaging. 2020;51(1):164–74. [PubMed: 31215107]
37. Onishi N, Sadinski M, Hughes MC, et al. Ultrafast dynamic contrast-enhanced breast MRI may generate prognostic imaging markers of breast cancer. Breast Cancer Res. 2020;22(1):58. [PubMed: 32466799]
38. Lo RC, Bensley RP, Hamdan AD, et al. Gender differences in abdominal aortic aneurysm presentation, repair, and mortality in the Vascular Study Group of New England. J Vasc Surg. 2013;57(5):1261–8, 8 e1-5. [PubMed: 23384493]
39. Gasser TC. Biomechanical Rupture Risk Assessment: A Consistent and Objective Decision-Making Tool for Abdominal Aortic Aneurysm Patients. Aorta (Stamford). 2016;4(2):42–60. [PubMed: 27757402]
40. Wang N, Christodoulou AG, Xie Y, et al. Quantitative 3D dynamic contrast-enhanced (DCE) MR imaging of carotid vessel wall by fast T1 mapping using Multitasking. Magn Reson Med. 2019;81(4):2302–14. [PubMed: 30368891]

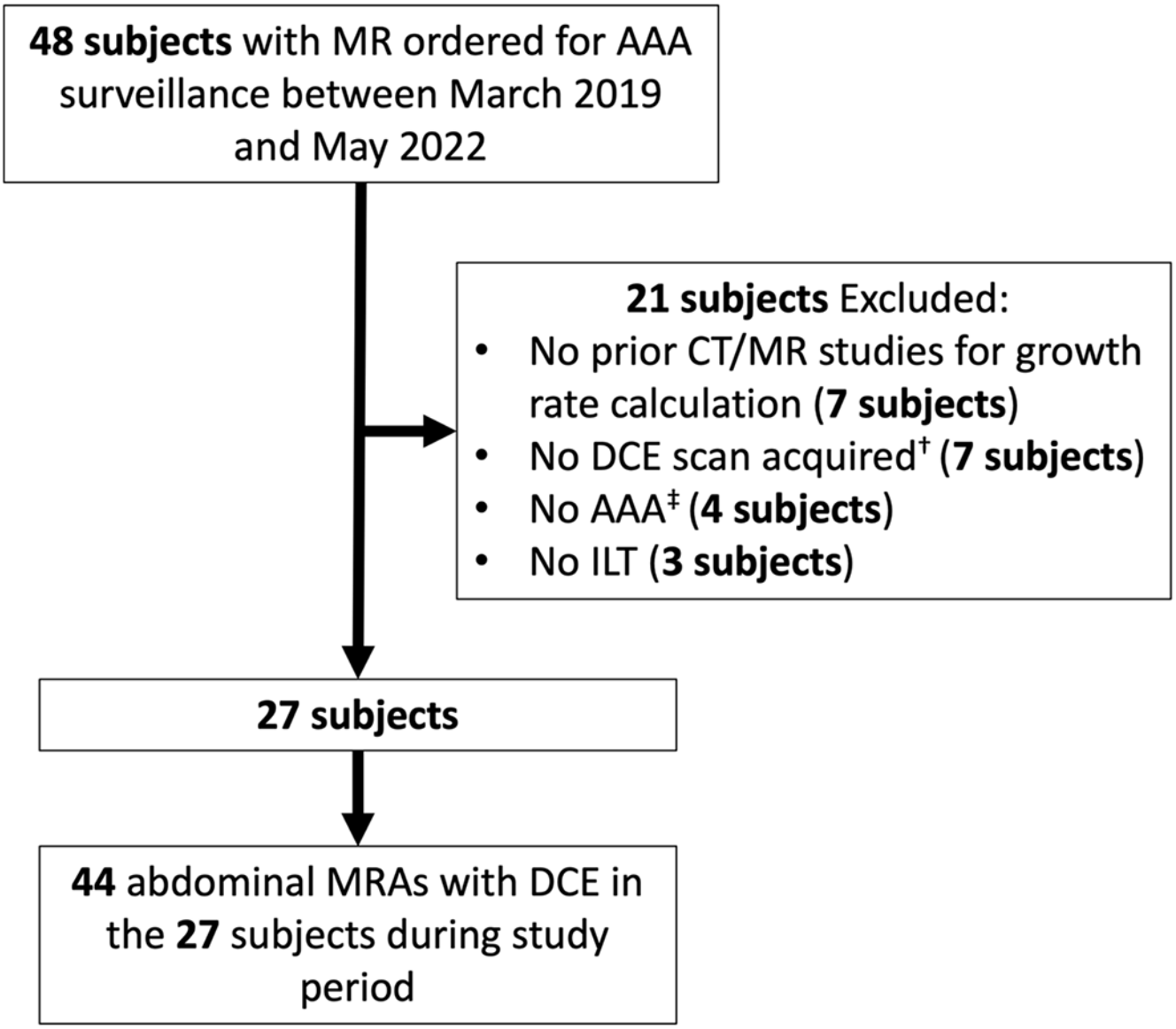

FIGURE 1:
Study inclusion flow chart. †Imaged with MRA protocol that did not include DCE. ‡Two subjects had only iliac aneurysms, and 2 subjects had <3.0 cm abdominal aortic size.

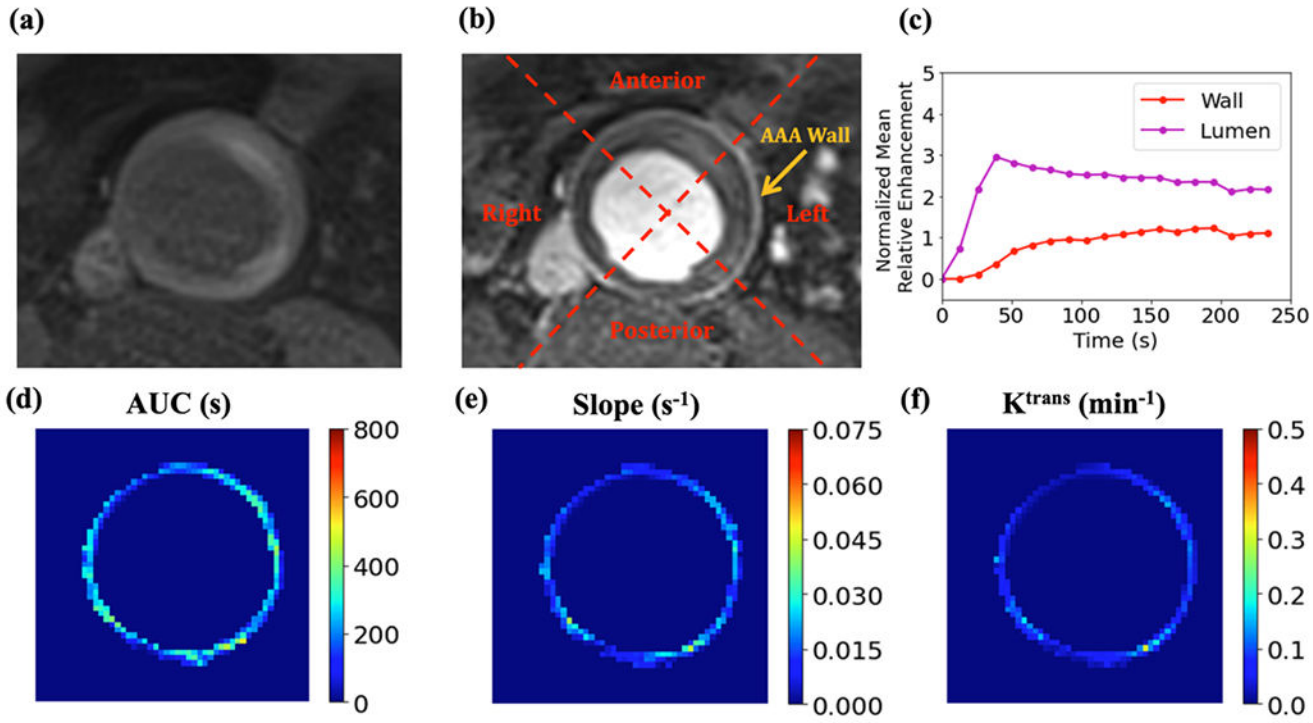

FIGURE 2:

Patient with AAA and slow growth rate of 1 mm/year. DCE images of AAA before (a) and after (b) contrast arrival. DCE measurements of the wall were averaged over the entire wall as well over each of the 4 anatomic quadrants separately (b). Normalized mean relative enhancement of the AAA wall and lumen for this patient (c). Voxel-wise maps of the AAA wall of this patient of normalized mean relative enhancement AUC from contrast arrival to 4 min (d) and slope from contrast arrival to 1 min (e), as well as K^{trans} (f).

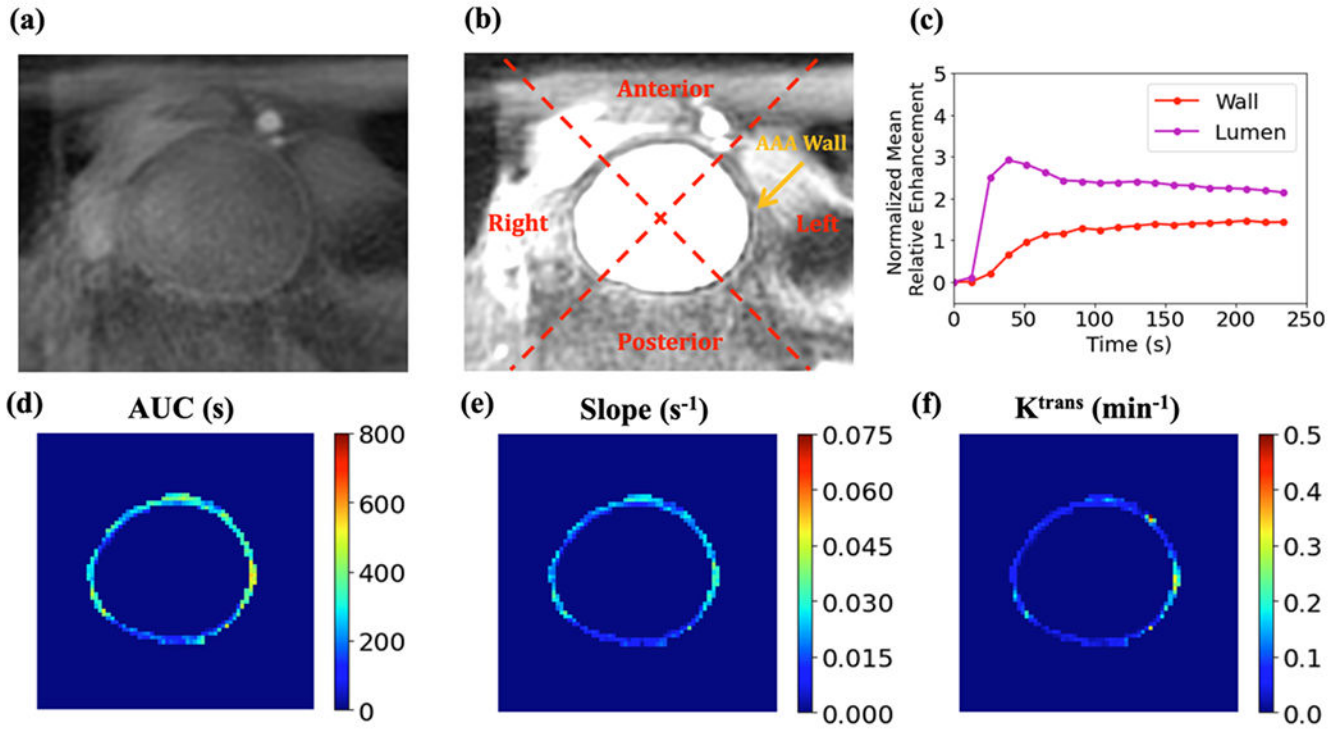

FIGURE 3:
Patient with AAA and fast growth rate of 5 mm/year. Panels (a)-(f) as in Figure 1.

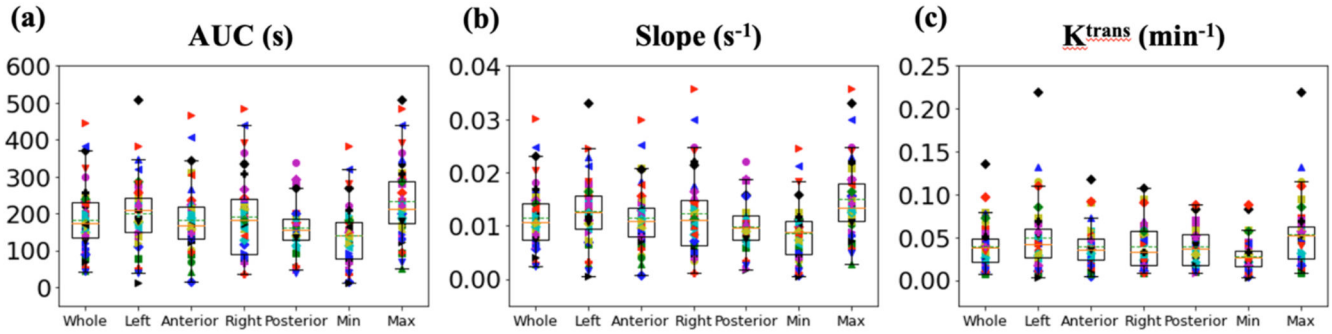

FIGURE 4:

Boxplots of AAA wall enhancement AUC up to 4 min (a), slope up to 1 min (b) and K^{trans} (c) of: the whole AAA wall, each of the four quadrants individually, and the minimum and maximum value across the 4 quadrants. Symbol color and shape represent individual DCE scans. Mean and median values are represented respectively by dashed green and solid orange horizontal lines within the boxes.

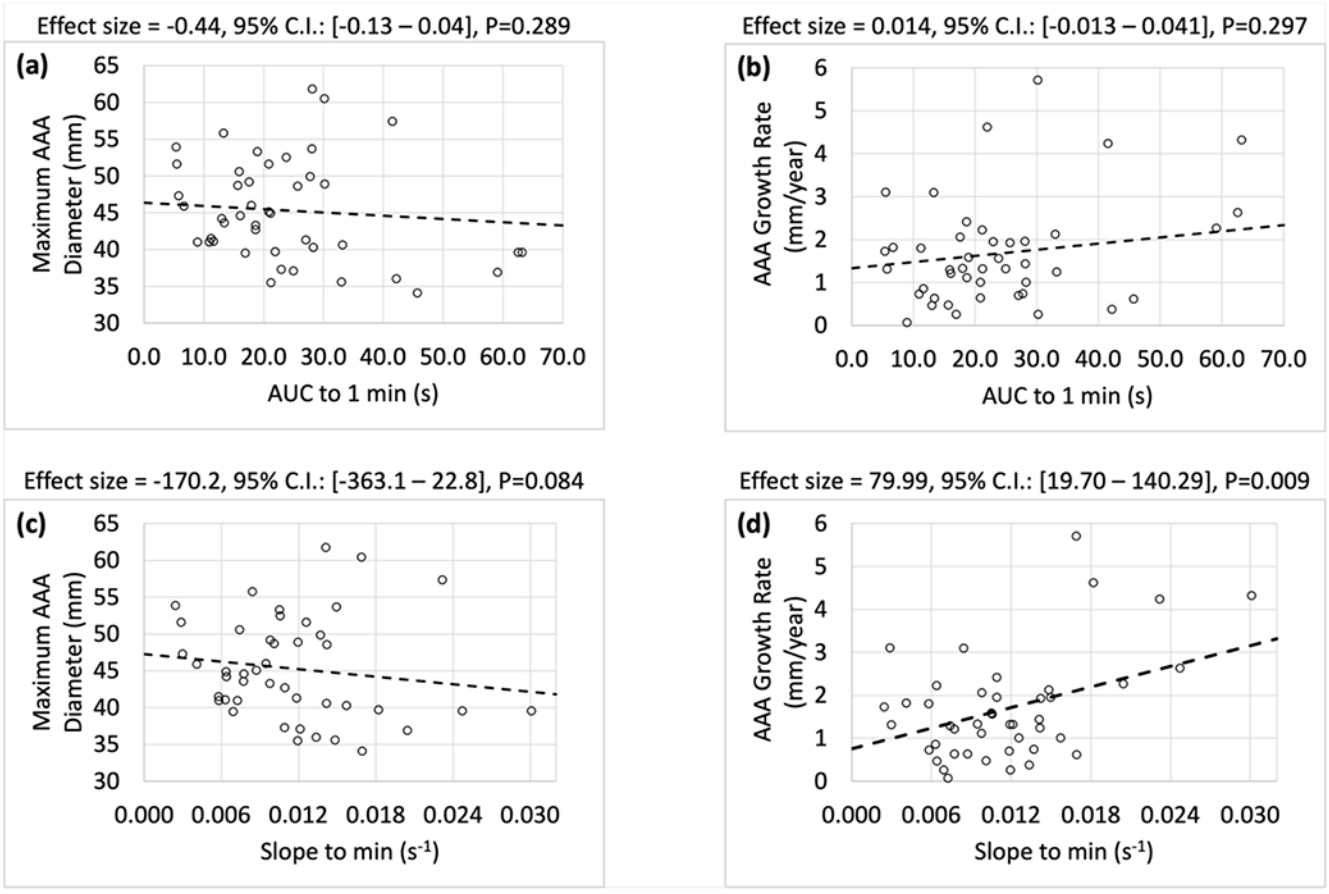

FIGURE 5:

Association of early AUC (contrast arrival to 1 min) and initial slope (contrast arrival to 1 min) with AAA maximum diameter (left-hand plots) and growth rate (right-hand plots) accounting for data clustering. C.I.: Confidence interval.

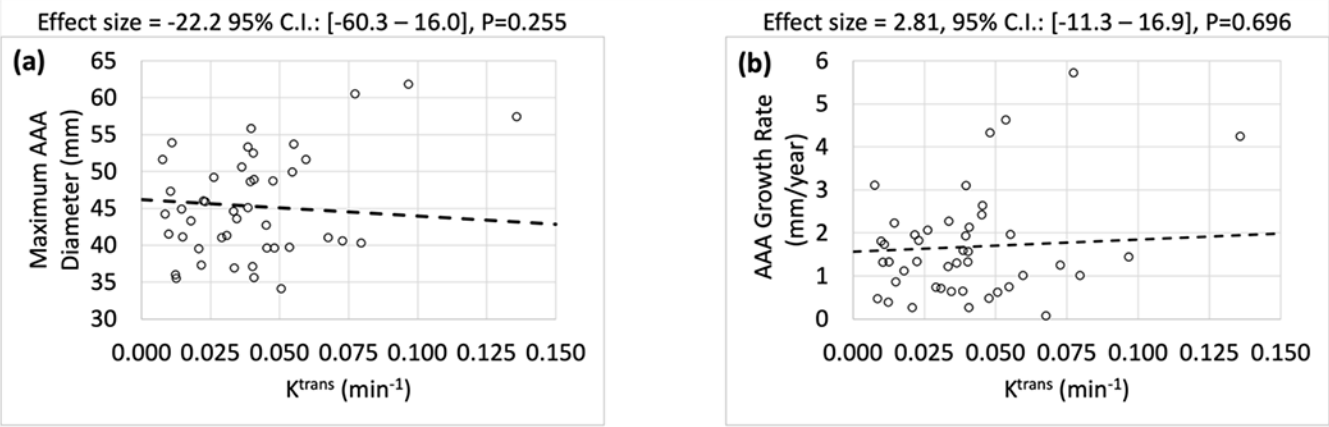

FIGURE 6:

Association between K^{trans} and AAA maximum diameter (a) and growth rate (b) accounting for data clustering. C.I.: Confidence interval.

TABLE 1.

Demographic information of the 27 AAA patients.

		N (%)
Male Sex		27 (100%)
Age (years)		76 ± 5.3
HTN		21 (77.8%)
HLD		25 (92.6%)
DM		9 (33.3%)
Smoker	Never	13 (48.2%)
	Former	9 (33.3%)
	Current	5 (18.5%)

M = Male; HTN = Hypertension; HLD = Hypersensitivity Lung Disease; DM = Diabetes Mellitus.

TABLE 2.

Heterogeneity of DCE measurements assessed via linear mixed effect models between DCE anterior-posterior and left-right aspect average measurements and the corresponding side of the measurement, with the anterior-posterior group as the reference.

		Coefficient	Standard Error	P value
Slope	Intercept (Reference A/P group)	0.011	0.001	<0.001
	L/R group	0.002	0.0006	0.008
AUC 1 min	Intercept (Reference A/P group)	23.36	2.679	<0.001
	L/R group	3.086	1.249	0.021
AUC 4 min	Intercept (Reference A/P group)	182.2	15.71	<0.001
	L/R group	24.94	8.845	0.010
K^{trans}	Intercept (Reference A/P group)	0.041	0.005	<0.001
	L/R group	0.008	0.003	0.021

AUC: Area under the curve; A/P: Anterior/posterior quadrants; L/R: Left/right quadrants.

TABLE 3.

Effect of DCE measurements on AAA growth rate after controlling for maximum AAA diameter.

	Coefficient	95% C.I.	P value
Slope	94.6	[39.4 – 149.9]	0.001
AUC 1 min	0.023	[−0.002 – 0.049]	0.076
AUC 4 min	0.006	[0.002 – 0.010]	0.002
K^{trans}	−2.12	[−15.9 – 11.6]	0.762

C.I. = Confidence interval; AUC: Area under the curve.

TABLE 4.

Interobserver bias, limits of agreement (LOA) and coefficient of variation (CoV) of DCE measurements in 10 studies.

	Bias	LOA	CoV
Slope	−0.0001 s^{-1}	[−0.0018 – 0.0016] s^{-1}	4.2%
AUC 1 min	−0.12 s	[−4.26 – 4.02] s	4.6%
AUC 4 min	1.4 s	[−25.8 – 23.01] s	3.8%
K^{trans}	−0.0011 min^{-1}	[−0.0042 – 0.0021] min^{-1}	2.8%